# CHAPTER IV
# RESULTS AND DISCUSSION

## 4.1 Photocatalyst Characterizations

### 4.1.1 TG-DTA Results

The TG-DTA curves were used to study the thermal decomposition behavior of the synthesized dried photocatalysts and to obtain their suitable calcination temperature. Figure 4.1 shows the TG-DTA curves of the dried $SrTiO_3$ and $SrTi_{0.97}Zn_{0.03}O_3$ gels. The DTA curves show four main exothermic regions. The first exothermic peak, with its position lower than 150 °C, is attributed to the removal of physisorbed water and ethanol molecules. The second exothermic peak region between 150 and 300 °C is attributed to the burnout of the LAHC surfactant molecules. The third exothermic region between 300 and 425 °C corresponds to the removal of organic remnants and chemisorbed water molecules (Hague *et al.*, 1994). The fourth exothermic region between 425 and 650°C corresponds to the crystallization process of the photocatalyst and the decomposition of solvent that is tightly bonded in the molecular level with Sr and Ti metals in the gel network (Puangpetch, *et al.*, 2008). The TG curves reveal that the calcination temperature of approximately 650 °C was sufficient for both the complete surfactant removal and the photocatalyst crystallization for both dried photocatalysts. Therefore, the calcination temperature in the range of 600 to 800 °C was used to investigate its effect on the physicochemical properties and the consequent photocatalytic phenol degradation activity of all the synthesized photocatalysts.

(a)

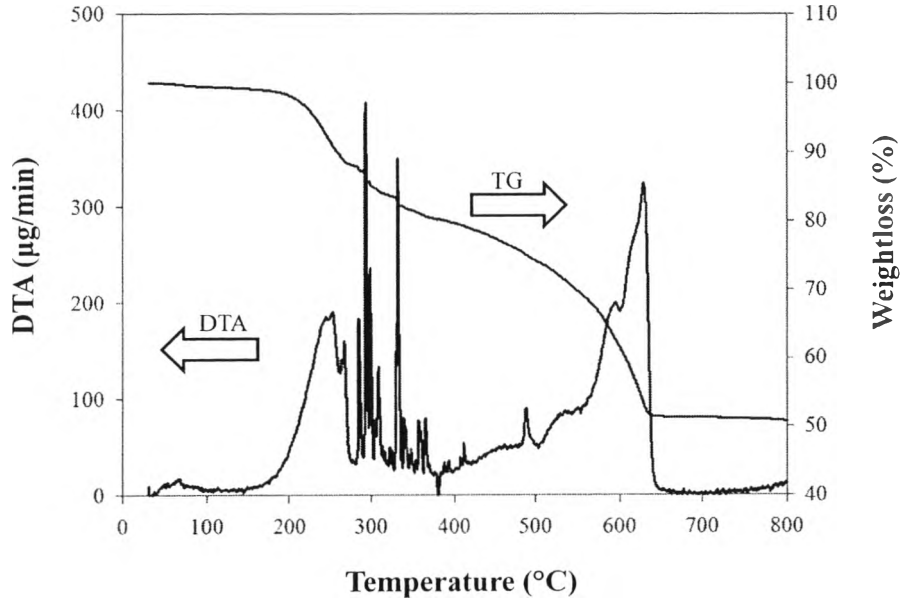


(b)

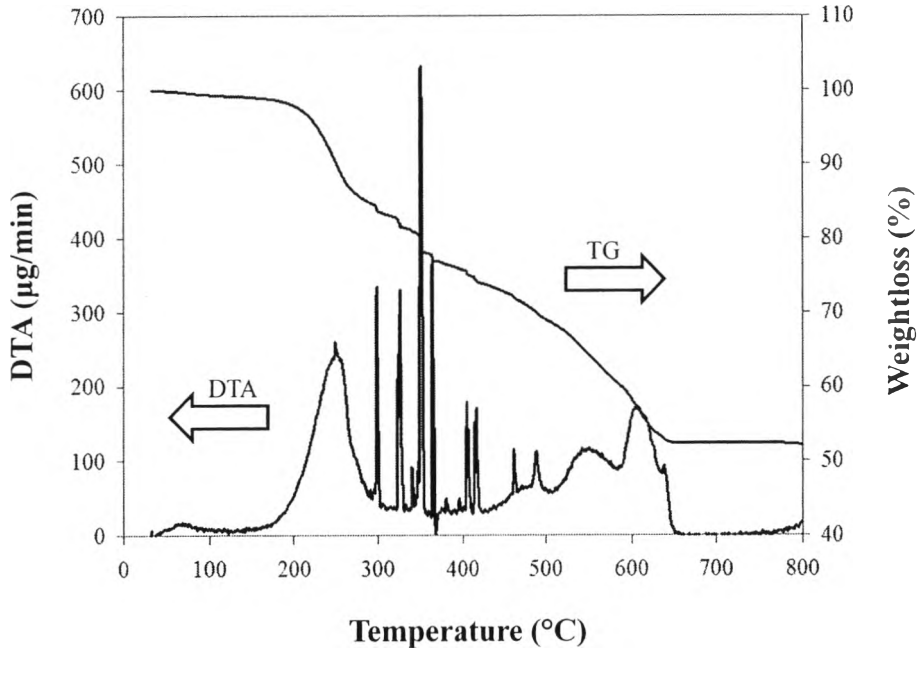


**Figure 4.1** TG-DTA curves of the dried synthesized (a) $SrTiO_3$ and (b) $SrTi_{0.97}Zn_{0.03}O_3$ photocatalysts.

4.1.2 $N_2$ Adsorption-Desorption Results

The $N_2$ adsorption-desorption analysis was used to verify the mesoporosity of the studied photocatalysts. The shape of the isotherms exhibits the characteristic behavior of the structure of powder, which is composed of an assembly of particles with large open packing. The adsorption-desorption isotherms of the synthesized $SrTiO_3$, $SrTi_{0.97}Zn_{0.03}O_3$, and 0.5 wt.% Pt-loaded $SrTi_{0.97}Zn_{0.03}O_3$ (which gave the highest photocatalytic activity, as shown later) photocatalysts calcined at 700 °C are comparatively exemplified in Figures 4.2 and 4.3. The isotherms of the photocatalysts exhibit typical IUPAC type IV-like pattern with a hysteresis loop, which is the characteristic of mesoporous material (mesoporous size between 2 and 50 nm) according to the classification of IUPAC (Rouquerol *et al.*, 1999). The insets of Figures 4.2 and 4.3 show the pore size distributions calculated from the desorption branch of the isotherms. All the photocatalysts possess quite narrow pore size distributions entirely locating in the mesoporous region (between 2 and 50 nm), implying a good quality of the samples.

The textural properties obtained from $N_2$ adsorption-desorption isotherms, i.e. specific surface area, mean mesopore diameter, and total pore volume, of all the investigated photocatalysts are summarized in Table 4.1. The specific surface area and total pore volume of the synthesized $SrTi_xZn_{1-x}O_3$ photocatalysts calcined at 700 °C tended to initially increase with increasing Zn content to 3 mol% (i.e. $SrTi_{0.97}Zn_{0.03}O_3$) and then adversely decreased with further increasing Zn content; however, the mean mesopore diameter remained almost unchanged. Hence, the synthesized mesoporous-assembled $SrTi_{0.97}Zn_{0.03}O_3$ photocatalyst was selected to further study the effect of calcination temperature in the range of 600 to 800 °C. As obviously seen, the specific surface area and total pore volume tended to increase with increasing calcination temperature from 600 to 700 °C and then decreased with further increasing calcination temperature to 800 °C; however, the mean mesopore diameter significantly decreased with increasing calcination temperature from 600 to 700 °C and then remained constant with further increasing calcination temperature to 800 °C. The results of textural properties of the metal-loaded $SrTi_{0.97}Zn_{0.03}O_3$ photocatalysts are shown in Table 4.2. It was interestingly found that the loaded metals could improve the specific surface area of $SrTi_{0.97}Zn_{0.03}O_3$ photocatalyst from

20.6 $m^2 \cdot g^{-1}$ to be higher than 30 $m^2 \cdot g^{-1}$. Moreover, with various Pt loadings, the results show that the specific surface area tended to increase with increasing Pt loading to reach a maximum value at 0.5 wt.% and then gradually decreased with further increasing Pt loading to 1 wt.%. However, the mean mesopore diameter remained almost unchanged at all Pt loadings in the investigated range.

(a)

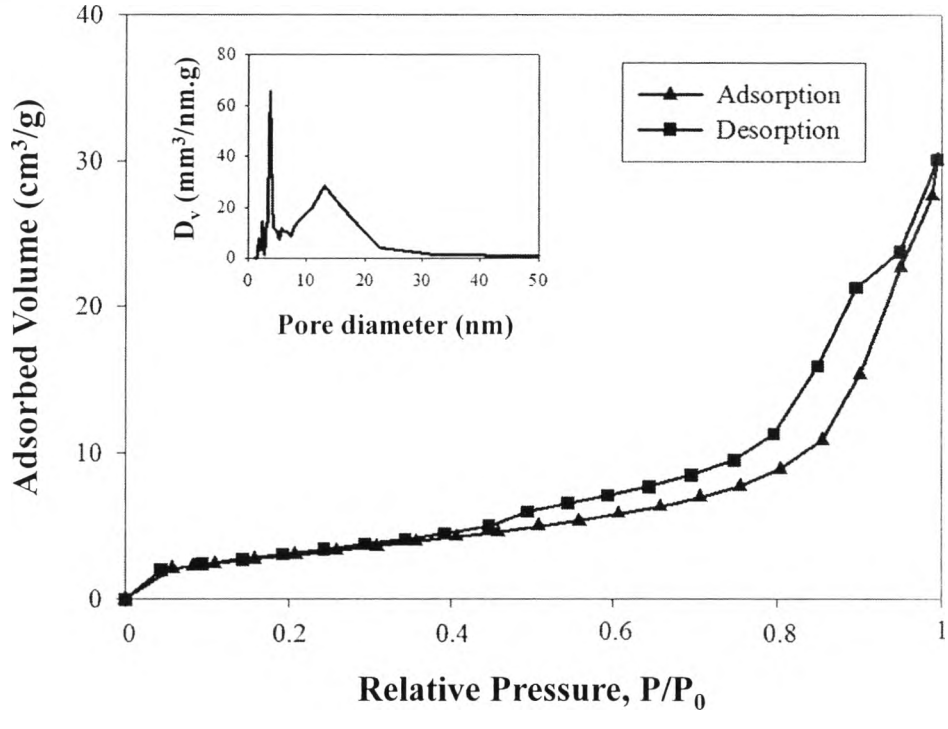


**Figure 4.2** $N_2$ adsorption-desorption isotherms and pore size distributions (inset) of the synthesized (a) $SrTiO_3$ and (b) $SrTi_{0.97}Zn_{0.03}O_3$ photocatalysts calcined at 700 °C.

(b)

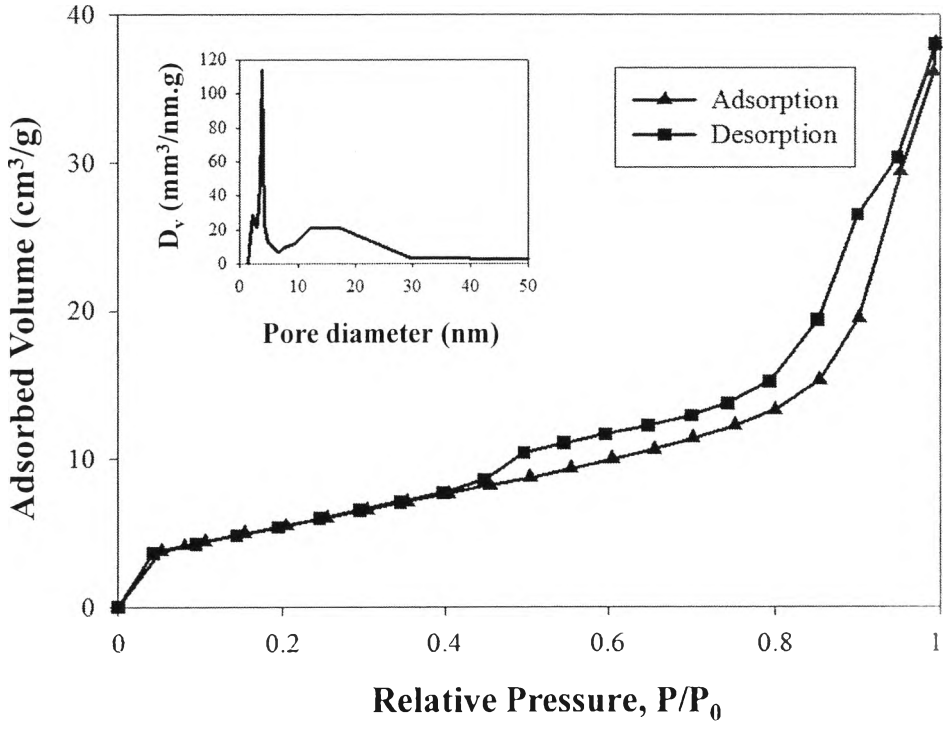


**Figure 4.2 (Continued)** $N_2$ adsorption-desorption isotherms and pore size distributions (inset) of the synthesized (a) $SrTiO_3$ and (b) $SrTi_{0.97}Zn_{0.03}O_3$ photocatalysts calcined at 700 °C.

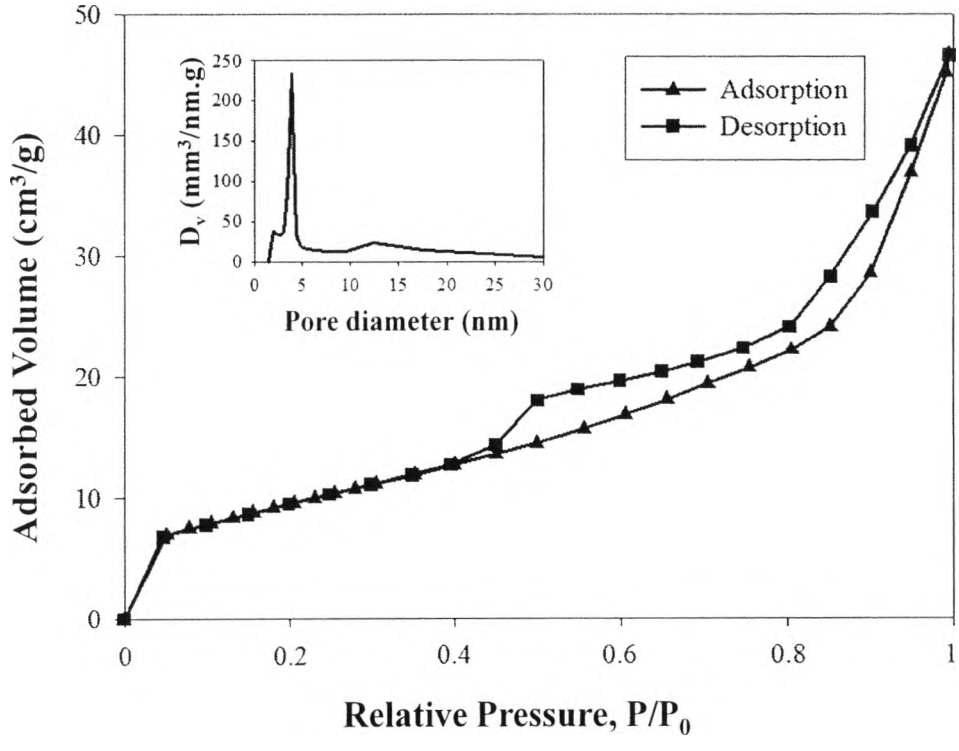


**Figure 4.3** $N_2$ adsorption-desorption isotherms and pore size distribution (inset) of the synthesized 0.5 wt.% Pt-loaded $SrTi_{0.97}Zn_{0.03}O_3$ photocatalyst calcined at 700 °C.

**Table 4.1** $N_2$ adsorption-desorption results of the synthesized mesoporous-assembled $SrTi_xZn_{1-x}O_3$ photocatalysts calcined at various temperatures

| Photocatalyst | Calcination temperature (°C) | Specific surface area ($m^2 \cdot g^{-1}$) | Mean mesopore diameter (nm) | Total pore volume ($cm^3 \cdot g^{-1}$) |
|---|---|---|---|---|
| $SrTiO_3$ | 700 | 11.5 | 3.90 | 0.042 |
| $SrTi_{0.97}Zn_{0.03}O_3$ | | 20.6 | 3.80 | 0.056 |
| $SrTi_{0.95}Zn_{0.05}O_3$ | | 7.7 | 3.78 | 0.024 |
| $SrTi_{0.93}Zn_{0.07}O_3$ | | 6.1 | 3.77 | 0.020 |
| $SrTi_{0.91}Zn_{0.09}O_3$ | | 5.2 | 3.77 | 0.018 |
| $SrTi_{0.97}Zn_{0.03}O_3$ | 600 | 9.03 | 9.59 | 0.020 |
| | 700 | 20.6 | 3.80 | 0.056 |
| | 800 | 11.6 | 3.80 | 0.036 |

**Table 4.2** $N_2$ adsorption-desorption results of the synthesized metal-loaded mesoporous-assembled $SrTi_{0.97}Zn_{0.03}O_3$ photocatalysts calcined at 700 °C

| Type of metal | Metal loading (wt.%) | Specific surface area ($m^2 \cdot g^{-1}$) | Mean mesopore diameter (nm) | Total pore volume ($cm^3 \cdot g^{-1}$) |
|---|---|---|---|---|
| - | - | 20.6 | 3.80 | 0.056 |
| Ag | 0.5 | 33.0 | 3.80 | 0.063 |
| Cu | 0.5 | 30.0 | 3.81 | 0.058 |
| Pt | 0.25 | 33.0 | 3.82 | 0.067 |
| | 0.5 | 35.1 | 3.79 | 0.057 |
| | 0.75 | 34.8 | 3.83 | 0.069 |
| | 1 | 34.4 | 3.81 | 0.072 |

4.1.3 XRD Results

The XRD patterns of the mesoporous-assembled $SrTi_xZn_{1-x}O_3$ photocatalysts with different Ti-to-Zn molar ratios calcined at 700 °C are shown in Figure 4.4. The dominant crystalline peaks of the cubic $SrTiO_3$ phase were observed at $2\theta$ of about 32.4°, 39.9°, 46.4°, 57.8°, 67.8°, and 77.2°, which represent the indices of (110), (111), (200), (211), (220), and (310) planes (Smith, 1960), respectively. For the (110) plane at $2\theta$ of 32.4°, the crystalline peak gradually shifted to a lower diffraction angle with increasing Zn content, confirming the presence of Zn in the form of solid solution in the synthesized $SrTi_xZn_{1-x}O_3$ photocatalysts. Figure 4.5 comparatively shows the XRD patterns of the mesoporous-assembled $SrTi_{0.97}Zn_{0.03}O_3$ photocatalysts calcined at various temperatures between 600 and 800 °C. When increasing the calcination temperature, all the crystalline peaks became sharper due to the crystallite growth. However, the presence of any diffraction peaks of the investigated metals (i.e. Ag, Cu, and Pt) loaded on the $SrTi_{0.97}Zn_{0.03}O_3$ photocatalyst could not be clearly observed from the XRD patterns, as shown in Figure 4.6. This is mainly because of their low loading contents of less than 1 wt.%.

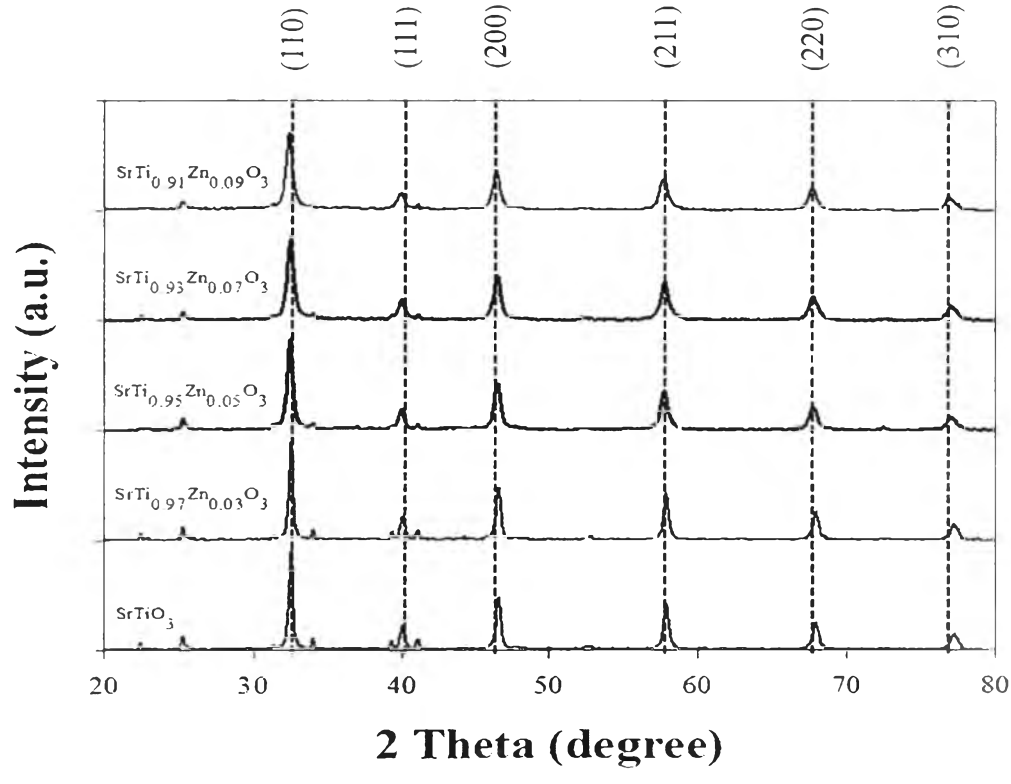


**Figure 4.4** XRD patterns of the mesoporous-assembled $SrTi_xZn_{1-x}O_3$ photocatalysts calcined at 700 °C.

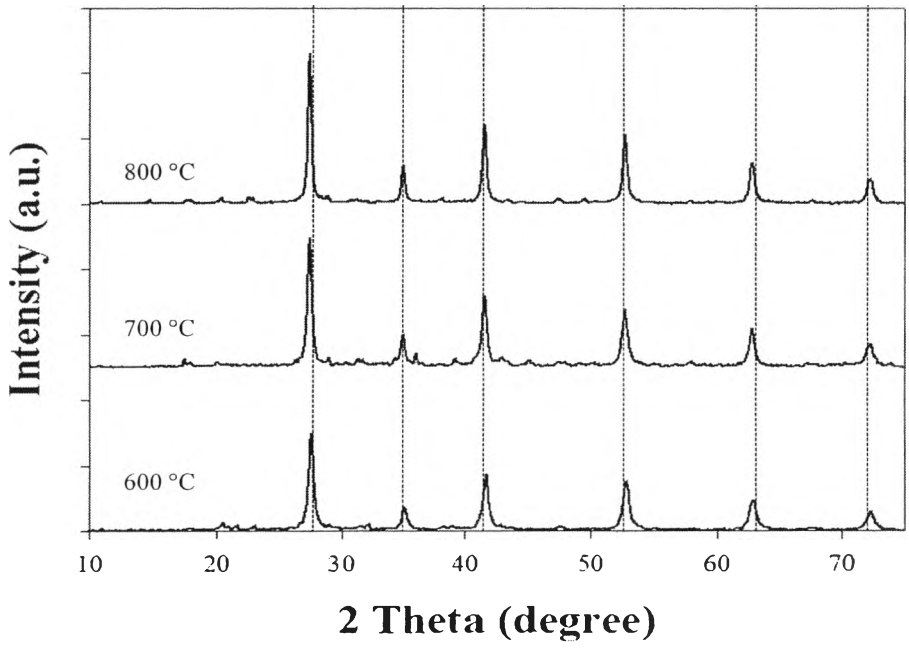


**Figure 4.5** XRD patterns of the mesoporous-assembled $SrTi_{0.97}Zn_{0.03}O_3$ photocatalysts calcined at various temperatures.

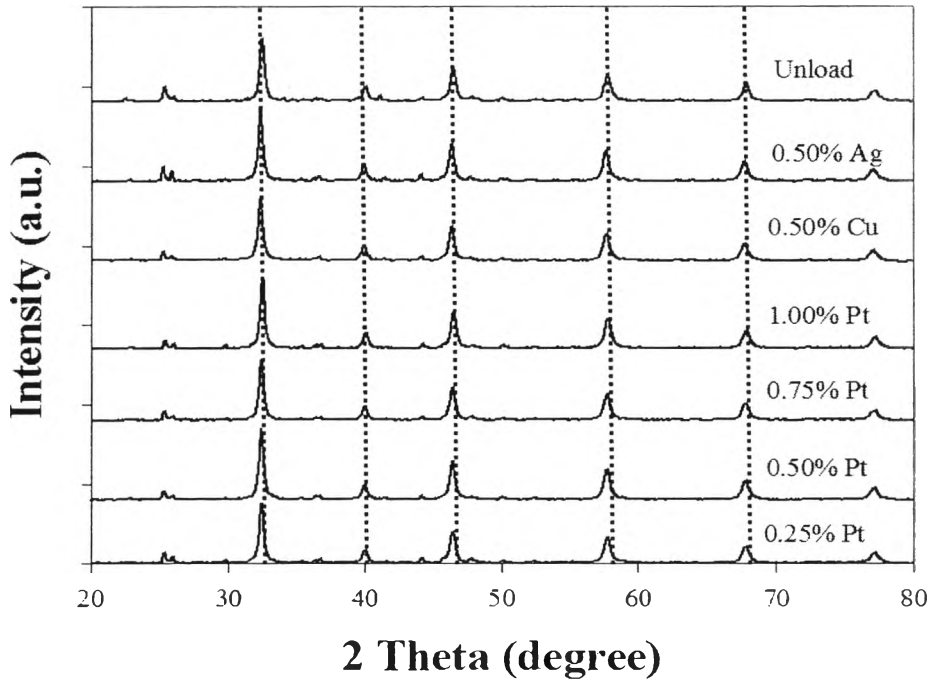


**Figure 4.6** XRD patterns of the mesoporous-assembled $SrTi_{0.97}Zn_{0.03}O_3$ photocatalysts without and with metal loadings calcined at 700 °C.

**Table 4.3** Crystallite size results of the synthesized mesoporous-assembled $SrTi_xZn_{1-x}O_3$ photocatalysts calcined at various temperatures

| Photocatalyst | Calcination temperature (°C) | Crystallite size (nm) |
|---|---|---|
| $SrTiO_3$ | 700 | 27.03 |
| $SrTi_{0.97}Zn_{0.03}O_3$ | | 21.87 |
| $SrTi_{0.95}Zn_{0.05}O_3$ | | 20.89 |
| $SrTi_{0.93}Zn_{0.07}O_3$ | | 18.53 |
| $SrTi_{0.91}Zn_{0.09}O_3$ | | 17.99 |
| $SrTi_{0.97}Zn_{0.03}O_3$ | 600 | 19.00 |
| | 700 | 21.87 |
| | 800 | 26.25 |

**Table 4.4** Crystallite size results of the synthesized metal-loaded mesoporous-assembled $SrTi_{0.97}Zn_{0.03}O_3$ photocatalysts calcined at 700 °C

| Photocatalyst | Metal loading (wt.%) | Crystallite size (nm) |
|---|---|---|
| $SrTi_{0.97}Zn_{0.03}O_3$ | - | 21.87 |
| | 0.5% Ag | 23.19 |
| | 0.5% Cu | 21.10 |
| | 0.25% Pt | 21.21 |
| | 0.5% Pt | 22.87 |
| | 0.75% Pt | 20.73 |
| | 1% Pt | 22.32 |

The crystallite sizes of the photocatalysts were calculated from the line broadening of the most preferentially formed X-ray diffraction peak of each crystalline phase according to the Scherrer equation (Cullity, 1978) (Eq. 4.1):

$$L = \frac{k\lambda}{\beta \cos(\theta)} \tag{4.1}$$

where $L$ is the crystallite size, $k$ is the Scherrer constant usually taken as 0.89, $\lambda$ is the wavelength of the X-ray radiation (0.15418 nm for Cu Kα), $\beta$ is the full width at half maximum (FWHM) of the diffraction peak measured at $2\theta$, and $\theta$ is the diffraction angle. The crystallite sizes of the synthesized mesoporous-assembled $SrTi_xZn_{1-x}O_3$ photocatalysts are shown in Table 4.3. The results clearly reveal that the crystallite size of the $SrTi_xZn_{1-x}O_3$ photocatalysts decreased from 27 nm to 18 nm with increasing Zn content. On the other hand, it was observed that the crystallite size of the $SrTi_{0.97}Zn_{0.03}O_3$ photocatalyst increased from 19 nm to 26 nm as the

calcination temperature increased from 600 °C to 800 °C. However, the metal loadings in the investigated range up to 1 wt.% did not significantly affect the crystallite size of the $SrTi_{0.97}Zn_{0.03}O_3$ photocatalyst, as shown in Table 4.4.

### 4.1.4 UV-Visible Spectroscopy Results

UV-visible spectroscopy was used to examine the light absorption ability of all the synthesized photocatalysts. The UV-visible spectra of the mesoporous-assembled $SrTi_xZn_{1-x}O_3$ calcined at 700 °C, $SrTi_{0.97}Zn_{0.03}O_3$ photocatalyst calcined at 600-800 °C, and various metals-loaded $SrTi_{0.97}Zn_{0.03}O_3$ calcined at 700 °C are comparatively shown in Figure 4.7. The results of absorption onset wavelength and corresponding band gap energy of all the photocatalysts without and with metal loadings are summarized in Tables 4.5 and 4.6. The band gap energy ($E_g$, eV) was determined by extrapolating the absorption onset of the rising part to x-axis ($\lambda_g$, nm) of the plots, as shown by dotted lines in Figure 4.7, and calculating by Eq. (4.2)

$$E_g = \frac{1240}{\lambda_g} \tag{4.2}$$

where $\lambda_g$ is the wavelength (nm) of the exciting light. It can be seen that the band gap energy of the $SrTi_xZn_{1-x}O_3$ photocatalysts slightly increased with increasing Zn content, but the band gap energy of the $SrTi_{0.97}Zn_{0.03}O_3$ photocatalyst tended to decrease with increasing calcination temperature. All the loaded metals (Ag, Cu, and Pt) could contribute to the increase in light-harvesting ability of the $SrTi_{0.97}Zn_{0.03}O_3$ photocatalyst within the visible light region (wavelength > 400 nm). However, the visible light response of photocatalysts did not pose any significant effect on their photocatalytic activity in this work (Onsuratoom *et al.*, 2011). For the Pt-loaded $SrTi_{0.97}Zn_{0.03}O_3$ photocatalysts, the Pt loading slightly increased the band gap energy from 3.06 to 3.13 eV.

(a)

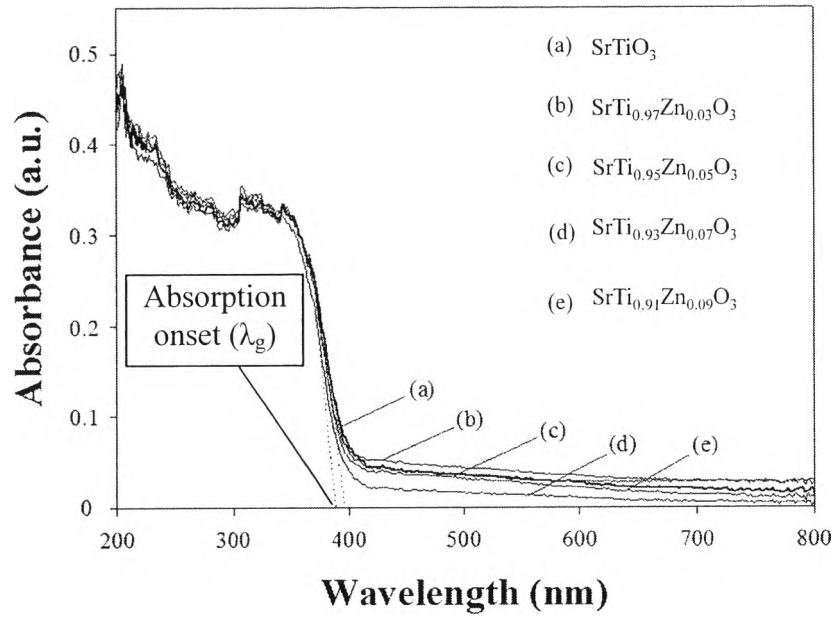


(b)

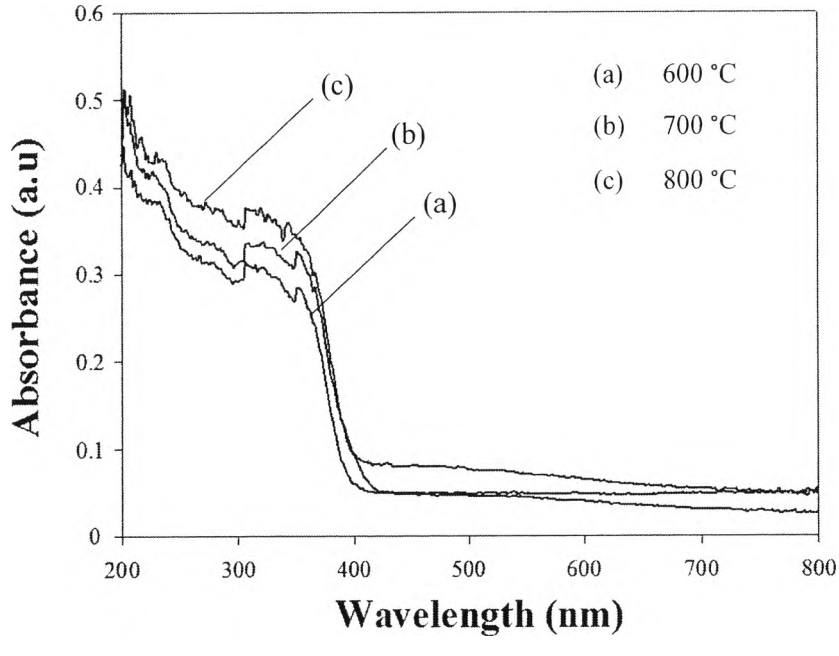


**Figure 4.7** UV-visible spectra of the mesoporous-assembled photocatalysts: (a) $SrTi_xZn_{1-x}O_3$ calcined at 700 °C, (b) $SrTi_{0.97}Zn_{0.03}O_3$ calcined at 600-800 °C, (c) various metals-loaded $SrTi_{0.97}Zn_{0.03}O_3$ calcined at 700 °C, and (d) Pt-loaded $SrTi_{0.97}Zn_{0.03}O_3$ with various Pt loadings calcined at 700 °C.

(c)

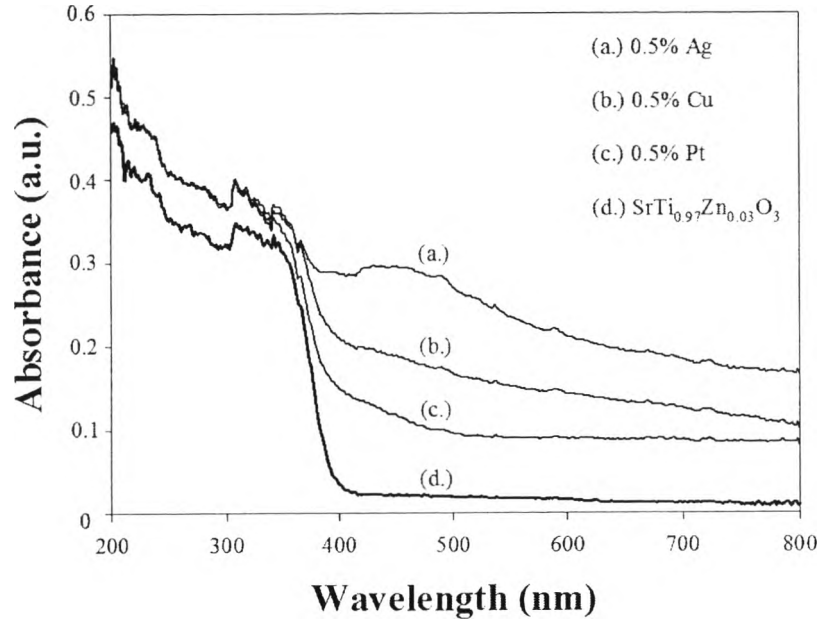


(d)

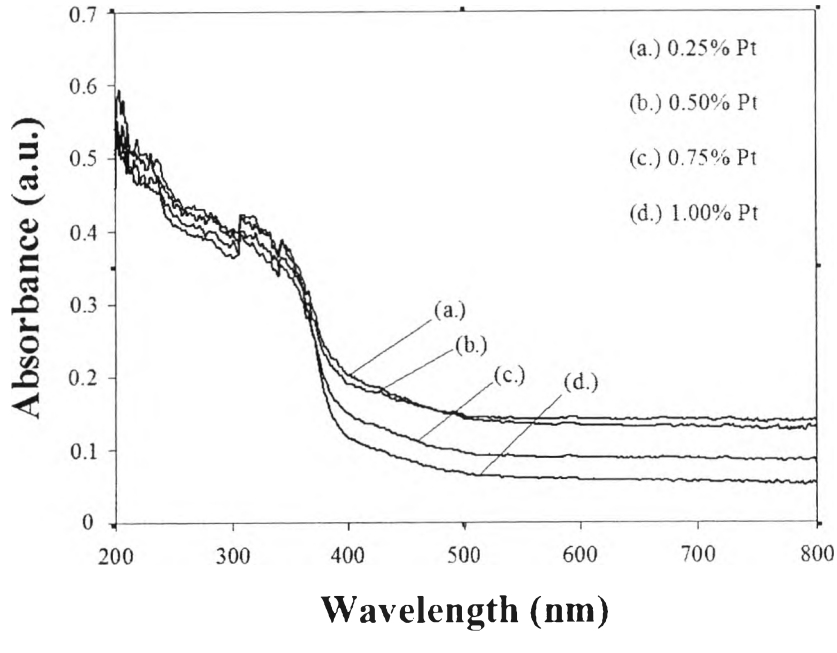


**Figure 4.7 (Continued)** UV-visible spectra of the mesoporous-assembled photocatalysts: (a) $SrTi_xZn_{1-x}O_3$ calcined at 700 °C, (b) $SrTi_{0.97}Zn_{0.03}O_3$ calcined at 600-800 °C, (c) various metals-loaded $SrTi_{0.97}Zn_{0.03}O_3$ calcined at 700 °C, and (d) Pt-loaded $SrTi_{0.97}Zn_{0.03}O_3$ with various Pt loadings calcined at 700 °C.

**Table 4.5** Absorption onset wavelength and band gap energy results obtained from UV-visible spectra of the synthesized mesoporous-assembled $SrTi_xZn_{1-x}O_3$ photocatalysts calcined at various temperatures

| Photocatalyst | Calcination temperature (°C) | Absorption onset wavelength, $\lambda_g$ (nm) | Band gap energy (eV) |
|---|---|---|---|
| $SrTiO_3$ | 700 | 397 | 3.12 |
| $SrTi_{0.97}Zn_{0.03}O_3$ | | 395 | 3.14 |
| $SrTi_{0.95}Zn_{0.05}O_3$ | | 393 | 3.15 |
| $SrTi_{0.93}Zn_{0.07}O_3$ | | 390 | 3.18 |
| $SrTi_{0.91}Zn_{0.09}O_3$ | | 388 | 3.20 |
| $SrTi_{0.97}Zn_{0.03}O_3$ | 600 | 380 | 3.26 |
| | 700 | 395 | 3.14 |
| | 800 | 394 | 3.14 |

**Table 4.6** Absorption onset wavelength and band gap energy results obtained from UV-visible spectra of the synthesized metal-loaded mesoporous-assembled $SrTi_{0.97}Zn_{0.03}O_3$ photocatalysts

| Photocatalyst | Metal loading (wt.%) | Absorption onset wavelength, $\lambda_g$ (nm) | Band gap energy (eV) |
|---|---|---|---|
| $SrTi_{0.97}Zn_{0.03}O_3$ | - | 395 | 3.14 |
| | 0.5% Ag | 410 | 3.02 |
| | 0.5% Cu | 410 | 3.02 |
| | 0.25% Pt | 405 | 3.06 |
| | 0.5% Pt | 400 | 3.10 |
| | 0.75% Pt | 396 | 3.13 |
| | 1% Pt | 396 | 3.13 |

### 4.1.5 SEM-EDX Results

The SEM images of the synthesized mesoporous-assembled $SrTiO_3$, $SrTi_{0.97}Zn_{0.03}O_3$, and 0.5 wt.% Pt-loaded $SrTi_{0.97}Zn_{0.03}O_3$ photocatalysts are shown in Figures 4.8(a), 4.9(a), and 4.10(a), respectively. The SEM images show the quite uniform-size particles of the samples in the form of aggregated clusters consisting of many nanoparticles. This nanoparticle aggregation can be possibly the cause of the mesoporous-assembled structure formation in the synthesized photocatalysts. The elemental distribution of the samples was investigated by the EDX mappings, as also shown in Figures 4.8(b), 4.9(b), and 4.10(b). The white dots in elemental mapping images indicate the existence and distribution of all the investigated components (Sr, Ti, Zn, O, and Pt) in the photocatalyst samples. It can be clearly seen that all elements of the $SrTiO_3$, $SrTi_{0.97}Zn_{0.03}O_3$, and 0.5 wt.% Pt-loaded $SrTi_{0.97}Zn_{0.03}O_3$ were well dispersed throughout the bulk samples. A quantity of each element in the synthesized photocatalysts was also obtained by the quantitative EDX elemental mapping analysis, as exemplified in Table 4.7 for the 0.5 wt.% Pt-loaded $SrTi_{0.97}Zn_{0.03}O_3$. The results show that the number of mole of all components based on 1 mole of Sr in the photocatalyst molecular structure was nearly the same as that in its theoretical chemical formula. For the loaded Pt component, its actual weight percentage was found to be approximately 0.48 wt.%, being almost equal to its nominal value of 0.5 wt.%.

(a)

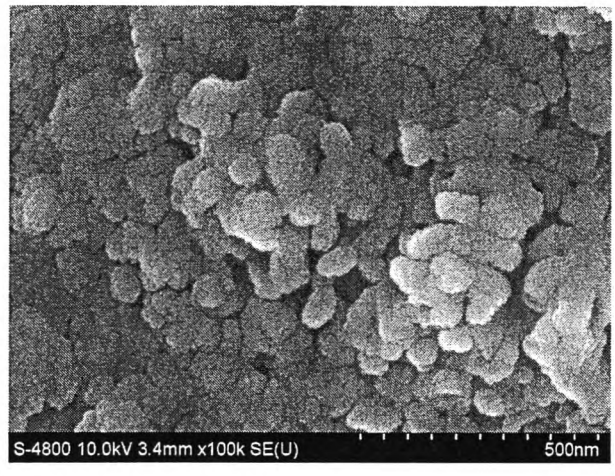


(b)

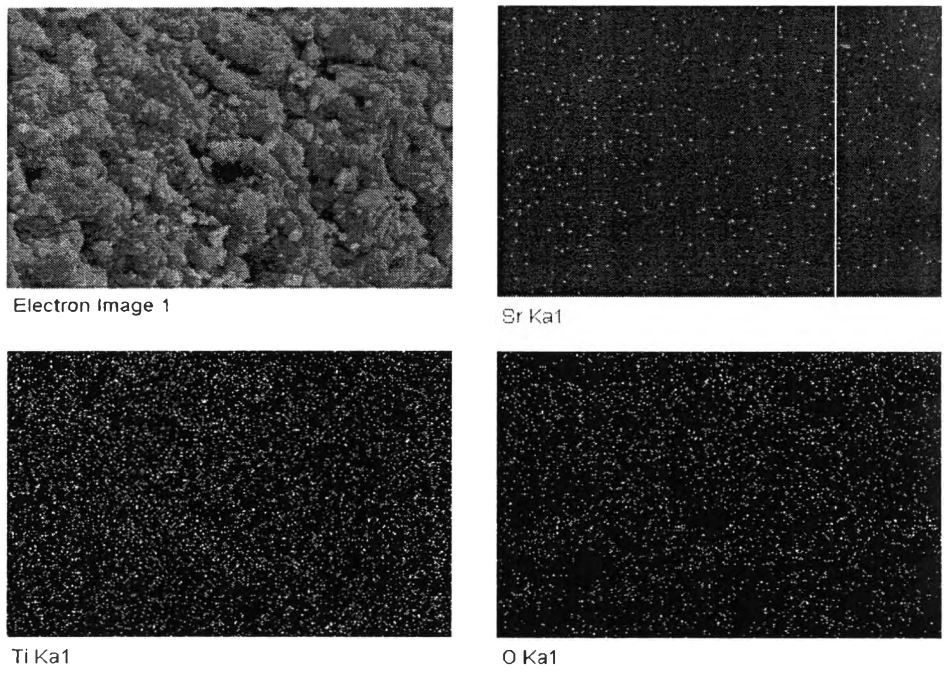


**Figure 4.8** SEM image (a) and EDX area mappings (b) of the synthesized mesoporous-assembled $SrTiO_3$ photocatalyst calcined at 700 °C.

(a)

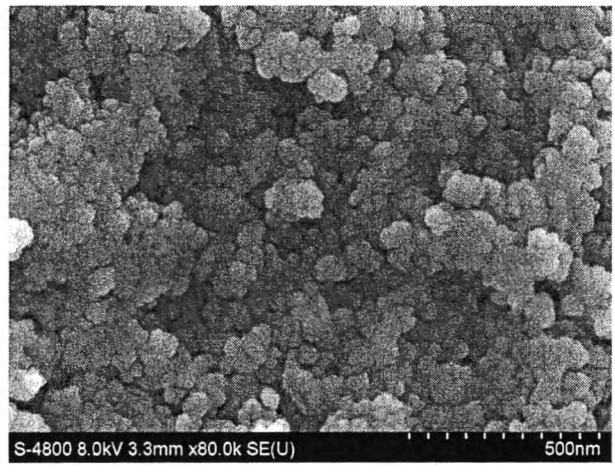


(b)

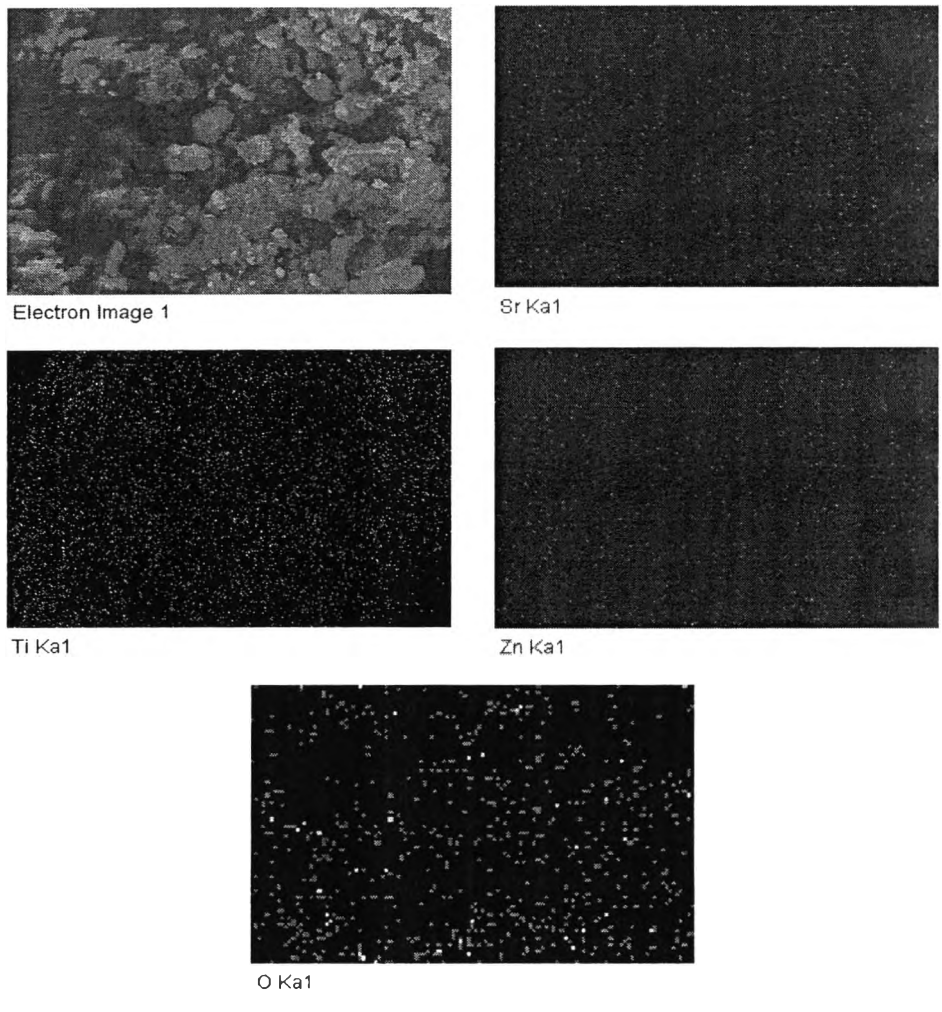


**Figure 4.9** SEM image (a) and EDX area mappings (b) of the synthesized mesoporous-assembled $SrTi_{0.97}Zn_{0.03}O_3$ photocatalyst calcined at 700 °C.

(a)

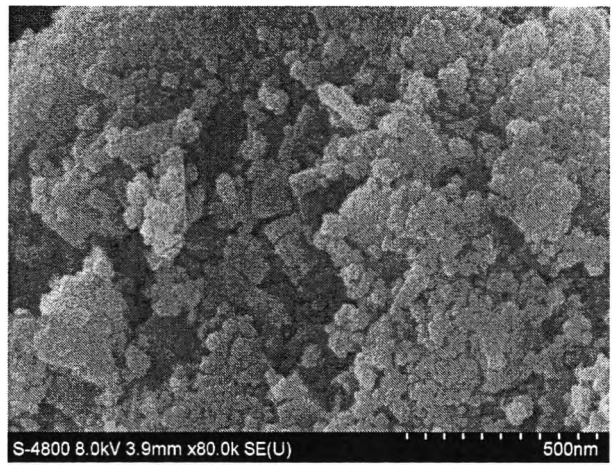


(b)

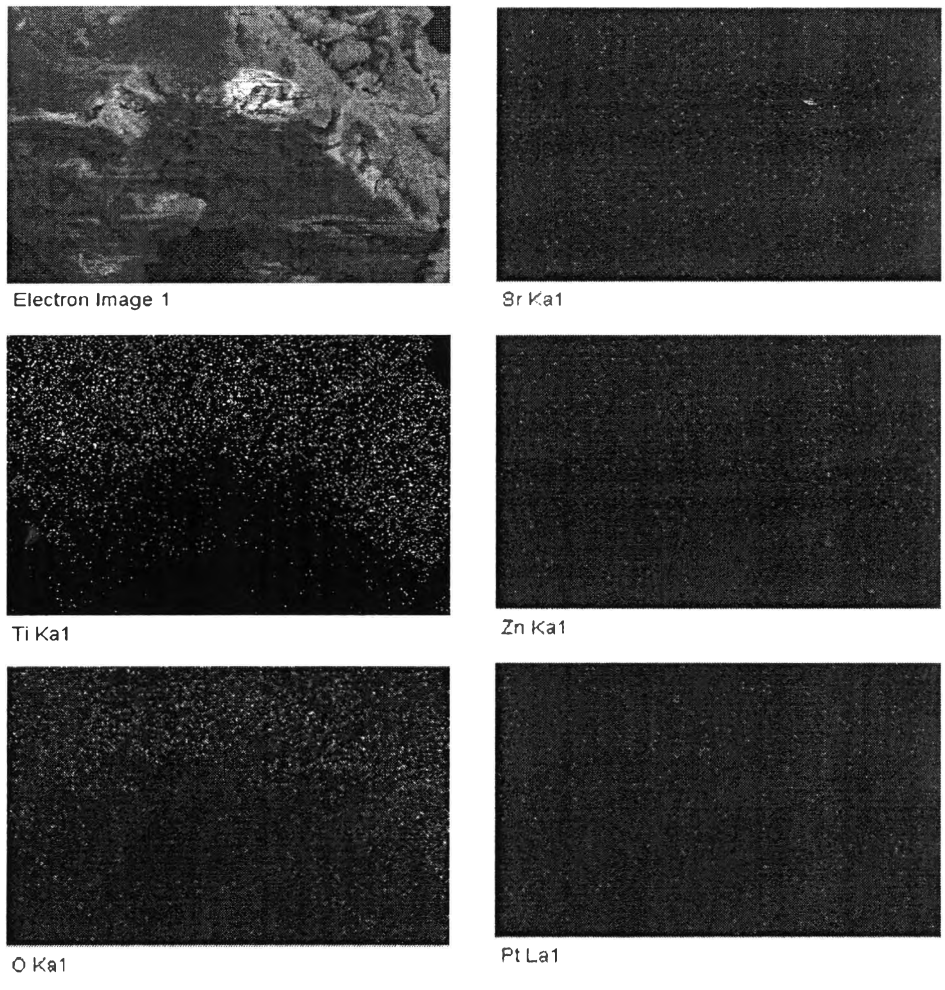


**Figure 4.10** SEM image (a) and EDX area mappings (b) of the synthesized 0.5 wt.% Pt-loaded mesoporous-assembled $SrTi_{0.97}Zn_{0.03}O_3$ photocatalyst calcined at 700 °C.

**Table 4.7** Quantitative EDX elemental mapping results of the 0.5 wt.% Pt-loaded mesoporous-assembled $SrTi_{0.97}Zn_{0.03}O_3$ photocatalyst calcined at 700 °C

| Photocatalyst | Element | Weight percentage (%) | Molar percentage (%) | Number of mole[(a)] |
|---|---|---|---|---|
| 0.5 wt.% Pt-loaded $SrTi_{0.97}Zn_{0.03}O_3$ | Pt | 0.48 | 0.08 | 0.01 |
| | Sr | 42.07 | 16.52 | 1.00 |
| | Ti | 21.87 | 15.72 | 0.95 |
| | Zn | 1.13 | 0.59 | 0.04 |
| | O | 34.45 | 74.10 | 4.48 |

[(a)] Based on 1 mole of Sr in the photocatalyst molecular structure

4.1.6 TEM-EDX Results

The morphology and particle size of the synthesized photocatalysts were investigated by the TEM analysis, as exemplified in Figure 4.11 for the $SrTiO_3$ and $SrTi_{0.97}Zn_{0.03}O_3$ calcined at 700 °C. The morphology of the $SrTiO_3$ and $SrTi_{0.97}Zn_{0.03}O_3$ photocatalysts is the cubic shape. The average particle sizes of the $SrTiO_3$ and $SrTi_{0.97}Zn_{0.03}O_3$ photocatalysts are in the range of 20-31 and 20-25 nm, respectively. These results suggest that the particle sizes of the photocatalysts are similar to their crystallite sizes calculated from the XRD patterns by the Scherrer equation, indicating a single crystalline characteristic. Besides, the EDX mapping analysis of the synthesized 0.5 wt.% Pt-loaded mesoporous-assembled $SrTi_{0.97}Zn_{0.03}O_3$ photocatalyst calcined at 700 °C was performed. As shown in Figure 4.12, the existence of the Pt nanoparticles on the $SrTi_{0.97}Zn_{0.03}O_3$ photocatalyst was clearly observed, as confirmed by the EDX mapping result. The average particle size of the Pt nanoparticles is approximately 15-23 nm.

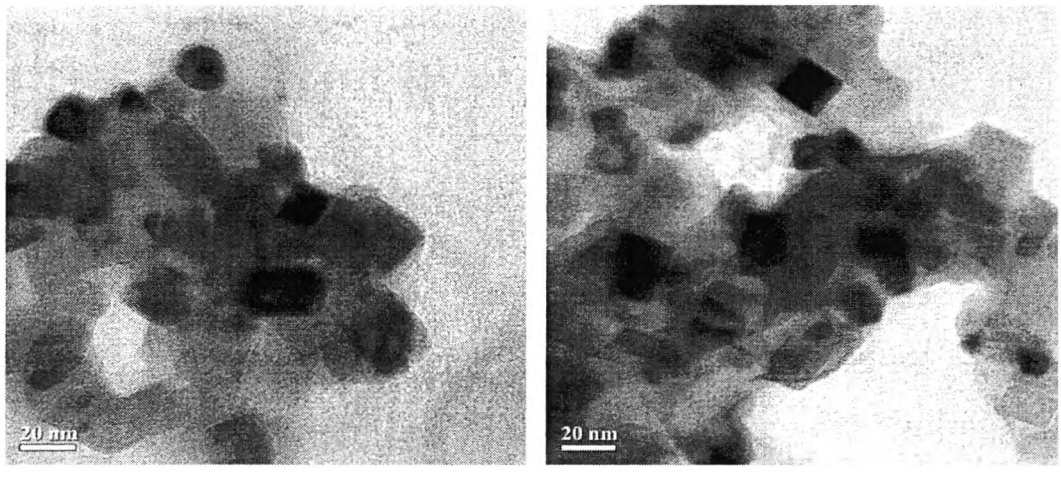


**Figure 4.11** TEM images of the synthesized (a) $SrTiO_3$ and (b) $SrTi_{0.97}Zn_{0.03}O_3$ photocatalysts calcined at 700 °C.

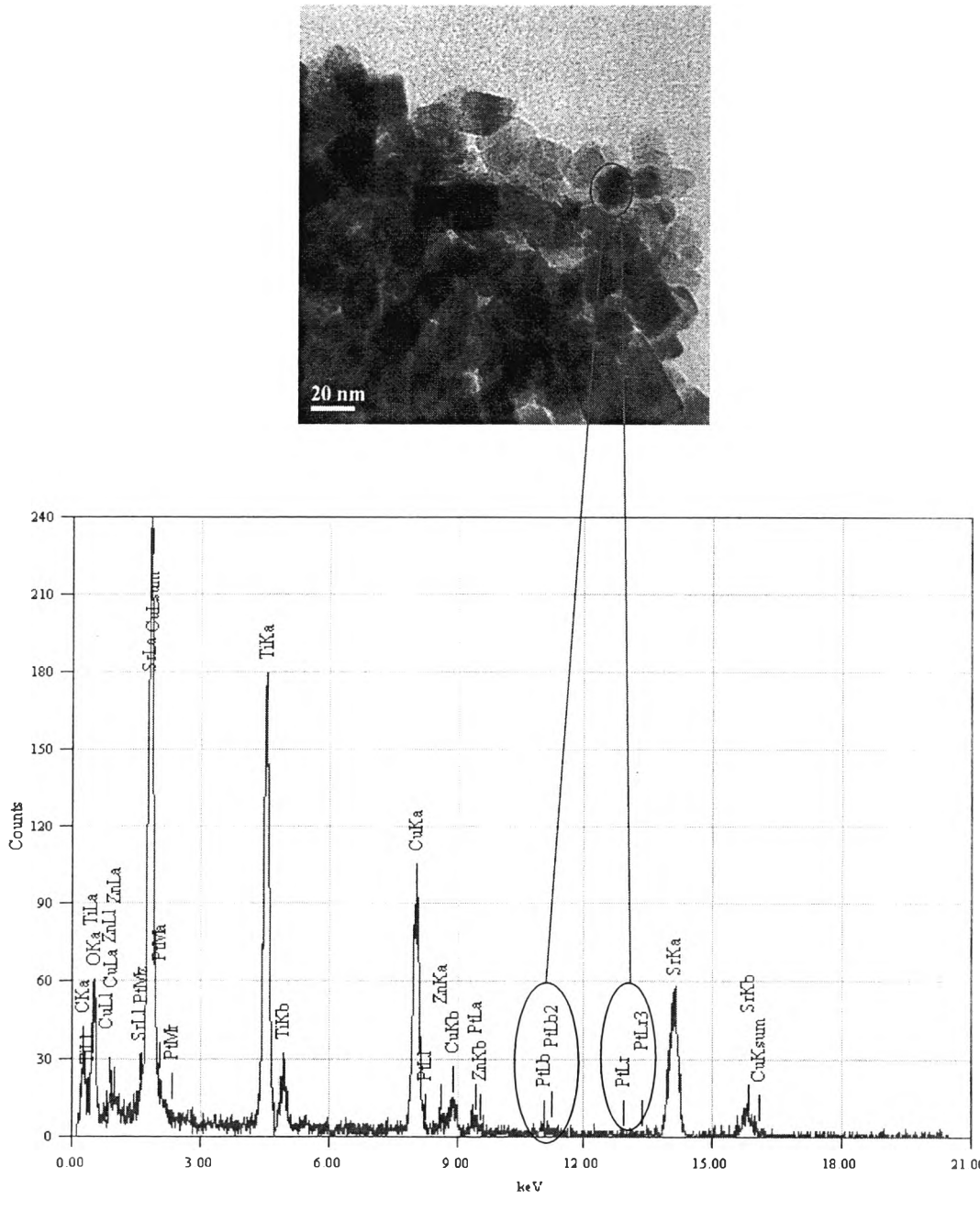


**Figure 4.12** TEM image and EDX elemental point mapping of the 0.5 wt.% Pt-loaded mesoporous-assembled $SrTi_{0.97}Zn_{0.03}O_3$ photocatalyst calcined at 700 °C.

4.1.7 $H_2$ Chemisorption Results

The $H_2$ chemisorption analysis was used to determine the dispersion of all loaded metals. As shown in Table 4.8, the results reveal that the type of loaded metals greatly affected the metal dispersion. For the case of various Pt loadings, the Pt dispersion increased with increasing Pt loading to reach a maximum value of 29.29% at 0.5 wt.%, and it decreased with further increasing Pt loading. This is possibly because the Pt nanoparticle agglomeration occurs at too high loadings.

**Table 4.8** Metal dispersion results of the synthesized metal-loaded mesoporous-assembled $SrTi_{0.93}Zn_{0.03}O_3$ photocatalysts

| Photocatalyst | Metal loading (wt.%) | Metal dispersion (%) |
|---|---|---|
| $SrTi_{0.93}Zn_{0.03}O_3$ | 0.5% Ag | 10.31 |
| | 0.5% Cu | 15.09 |
| | 0.25% Pt | 12.61 |
| | 0.5% Pt | 29.29 |
| | 0.75% Pt | 16.61 |
| | 1% Pt | 13.29 |

## 4.2 Photocatalytic Phenol Degradation Results

### 4.2.1 UV-Visible Spectroscopy Results

UV-visible spectroscopy was used to investigate the effects of various reaction parameters on the phenol degradation performance of all the synthesized $SrTi_xZn_{1-x}O_3$ photocatalysts. As colorimetrically determined with 4-aminoantipyrine (Franson, 1989), the UV-visible spectra of phenol solutions reveal the $\lambda_{max}$ value at 500 nm, as shown in Figure 4.13. The absorbances at this $\lambda_{max}$ value were then used to investigate the phenol degradation.

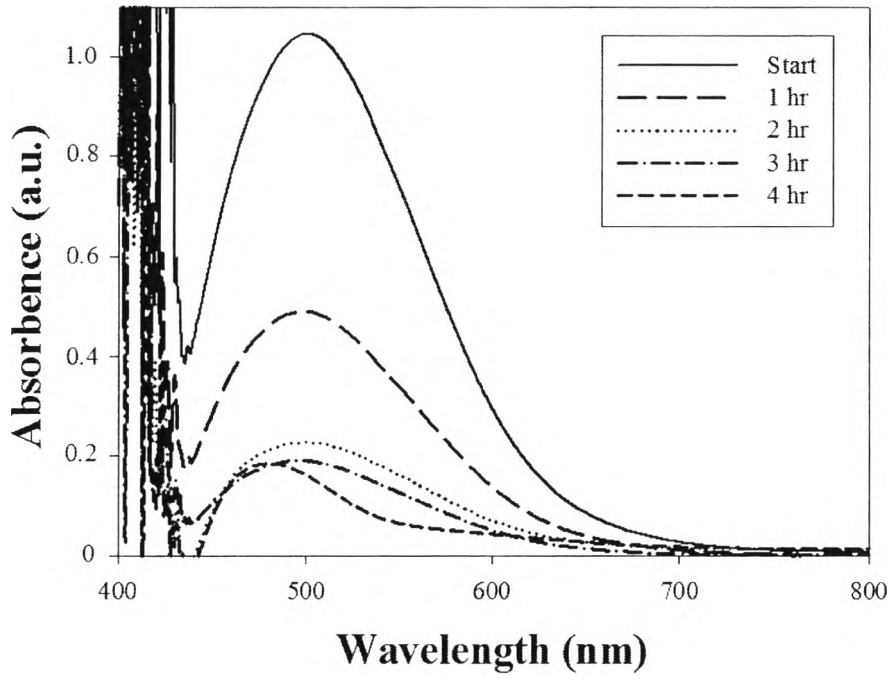


**Figure 4.13** UV-visible spectra of phenol solutions at various irradiation times.

4.2.2 Effect of Ti-to-Zn Molar Ratio

In this research, the mesoporous-assembled $SrTi_xZn_{1-x}O_3$ photocatalysts synthesized with various Ti-to-Zn molar ratios calcined at 700 °C were used to study the phenol degradation performance in order to find the suitable Ti-to-Zn molar ratio that exhibits the highest photocatalytic activity. The results of photocatalytic phenol degradation in terms of reaction rate constant (k) are shown in Figure 4.14. It can be observed that the reaction rate constant increased with increasing Zn content and reached a maximum value at 3 mol % (i.e. $SrTi_{0.97}Zn_{0.03}O_3$). However, it significantly decreased with further increasing Zn content higher than 3 mol%. Hence, the synthesized mesoporous-assembled $SrTi_{0.97}Zn_{0.03}O_3$ photocatalyst provided the highest photocatalytic activity (k = 0.808 $h^{-1}$). The photocatalytic activity results can be explained by the specific surface area results (Table 4.1) that the incorporation of Zn with its suitable content of 3 mol% enhanced the specific surface area of the $SrTi_{0.97}Zn_{0.03}O_3$ photocatalyst, implying its higher surface active reaction sites and lower probability of charge carrier recombination. However, the observed results of the decreased reaction rate constant at Zn contents higher than 3 mol% can be explained by their lower specific surface areas, leading to lower surface active reaction sites, as well as their very small crystallite sizes (Table 4.3), leading to higher probability of charge carrier recombination at both the surface and bulk traps (Sreethawong *et al.*, 2005). Therefore, the synthesized mesoporous-assembled $SrTi_{0.97}Zn_{0.03}O_3$ photocatalyst was selected for further experiments.

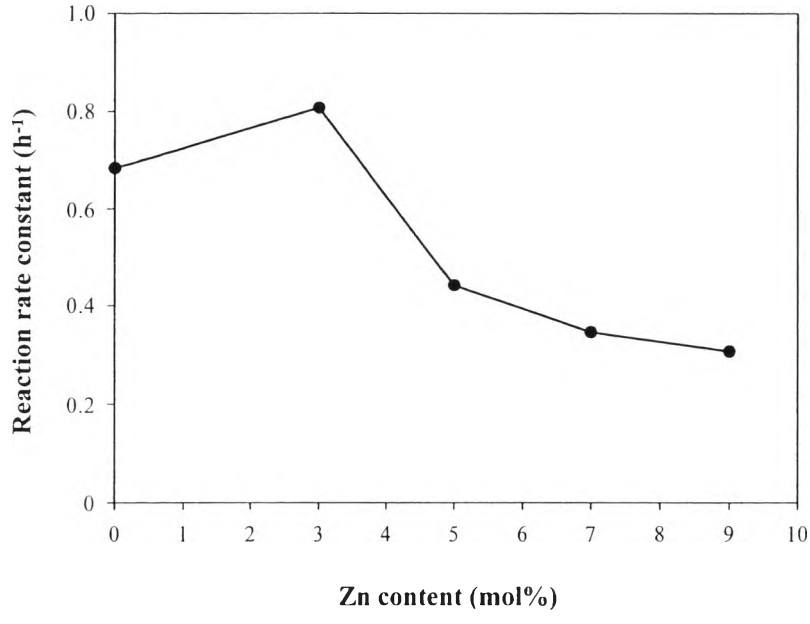


**Figure 4.14** Effect of Ti-to-Zn molar ratio in terms of Zn content on the reaction rate constant for phenol degradation of the synthesized mesoporous-assembled $SrTi_xZn_{1-x}O_3$ photocatalysts calcined at 700 °C (Photocatalyst, 1 g; total reaction mixture volume, 200 ml; initial phenol concentration, 40 mg/l; and irradiation time, 4 h).

4.2.3 Effect of Calcination Temperature

The photocatalytic activity results of the $SrTi_{0.97}Zn_{0.03}O_3$ photocatalyst calcined at various temperatures between 600 and 800 °C are shown in Figure 4.15. It was found that the reaction rate constant increased with increasing calcination temperature and reached a maximum value at 700 °C. However, when the calcination temperature exceeded 700 °C, the reaction rate constant decreased. These can be explained that an increase in the calcination temperature in the range of 600-700 °C led to an increase in the specific surface area (Table 4.1), which positively affected the photocatalytic activity. For the calcination temperature in the range of 700-800 °C, decreases in the specific surface area and band gap energy (Tables 4.1 and 4.5) may possibly increase the probability of the charge carrier recombination at the bulk traps. Therefore, the calcination temperature of 700 °C was considered as the optimum value to be used in further experiments.

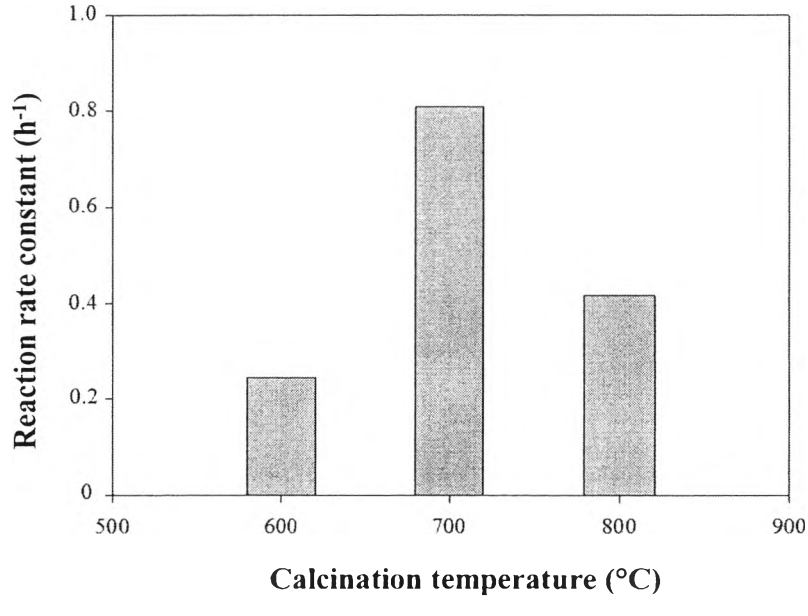


**Figure 4.15** Effect of calcination temperature on the reaction rate constant for phenol degradation of the synthesized mesoporous-assembled $SrTi_{0.97}Zn_{0.03}O_3$ photocatalyst (Photocatalyst, 1 g; total reaction mixture volume, 200 ml; initial phenol concentration, 40 mg/l; and irradiation time, 4 h).

### 4.2.4 Effect of Different Metal Types

In this part, the mesoporous-assembled $SrTi_{0.97}Zn_{0.03}O_3$ photocatalysts loaded with different 0.5 wt.% metal types (i.e. Ag, Cu, and Pt) were comparatively used for the photocatalytic activity testing. The results of the photocatalytic phenol degradation in terms of reaction rate constant of the photocatalysts are shown in Figure 4.16. It can be clearly observed that all of the metals had a positive effect on the photocatalytic activity of the mesoporous-assembled $SrTi_{0.97}Zn_{0.03}O_3$ photocatalysts. The loaded metals can help accelerate the electron transfer and act as electron-capturing sites after band gap excitation to prevent the charge carrier recombination. The captured electrons on the loaded metals can react with $O_2$ molecules adsorbed on the photocatalyst surface and dissolved in the solution, whereas the holes can more easily react with $H_2O$ molecules to generate several active species, e.g. $O_2^{\bullet-}$, $OH^{\bullet}$, and $OH_2^{\bullet}$, leading to the enhancement of the photocatalytic activity. However, the higher electronegativity of Pt nanoparticles possibly induces them to behave as more efficient active sites, which can hold electrons much better than the other metals, resulting in the highest photocatalytic activity of the Pt-loaded sample.

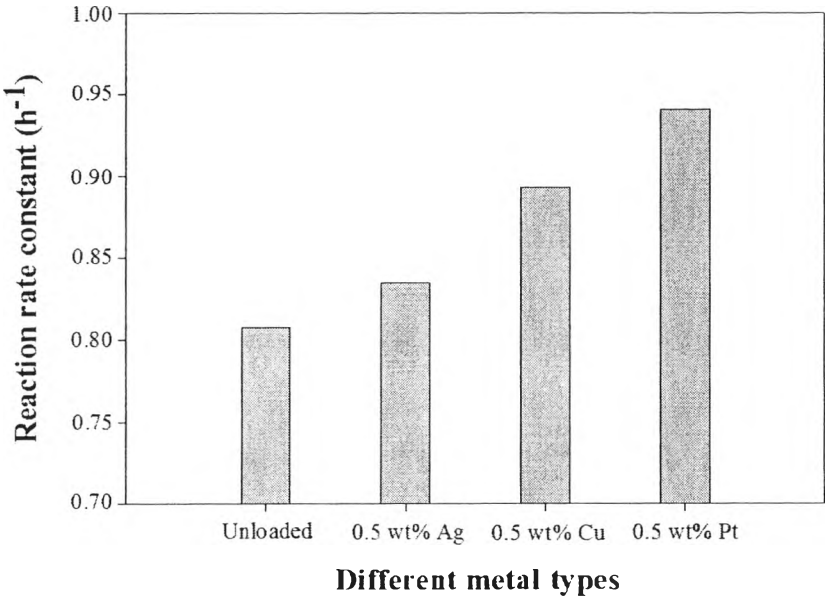


**Figure 4.16** Effect of different metal types on the reaction rate constant for phenol degradation of the synthesized metal-loaded mesoporous-assembled $SrTi_{0.97}Zn_{0.03}O_3$ photocatalysts calcined at 700 °C (Photocatalyst, 1 g; total reaction mixture volume, 200 ml; initial phenol concentration, 40 mg/l; and irradiation time, 4 h).

4.2.5 Effect of Pt Loading

The synthesized mesoporous-assembled $SrTi_{0.97}Zn_{0.03}O_3$ photocatalyst was used for further investigating the effect of Pt loading in the range of 0.25-1 wt.% on the photocatalytic phenol degradation. The results of the photocatalytic phenol degradation in terms of reaction rate constant are shown in Figure 4.17. It was found that the reaction rate constant increased with increasing Pt loading to 0.5 wt.%, which provided the highest reaction rate constant of 0.941 $h^{-1}$; however, it significantly decreased with further increasing Pt loading higher than 0.5 wt.%. It can be explained in that too much Pt loading resulted in a higher probability of the Pt nanoparticles to agglomerate and undesirably behave as recombination centers. This consequently led to a marked increase in the charge carrier recombination frequency because the average distance between trapping sites decreases by increasing the number and size of Pt nanoparticles confined within a photocatalyst particle (Sreethawong *et al.*, 2005). In overall, the optimum Pt loading for the present investigated system was considered to be 0.5 wt.%.

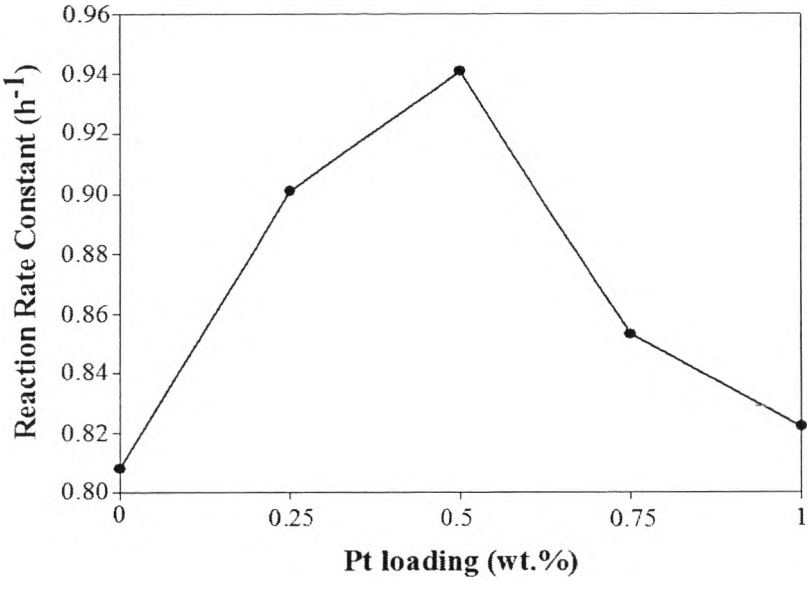


**Figure 4.17** Effect of Pt loading on the reaction rate constant for phenol degradation of the synthesized Pt-loaded mesoporous-assembled $SrTi_{0.97}Zn_{0.03}O_3$ photocatalysts calcined at 700 °C (Photocatalyst, 1 g; total reaction mixture volume, 200 ml; initial phenol concentration, 40 mg/l; and irradiation time, 4 h).

4.2.6 Effect of Dissolved Oxygen

The effect of dissolved oxygen on the photocatalytic phenol degradation performance of the 0.5 wt.% Pt-loaded $SrTi_{0.97}Zn_{0.03}O_3$ was further investigated. The dissolved oxygen in the phenol solution was detected by a DO meter. In case of no gas bubbling, the phenol solutions before and after the reaction had the dissolved oxygen values of 8.03 and 4.11 mg/l, respectively. Therefore, the effect of dissolved oxygen was investigated under the bubbling of different gases into the suspension. The dissolved oxygen values in the case of $N_2$ and $O_2$ bubblings were 0 and 35.5 mg/l, respectively. As shown Figure 4.18, the photocatalytic activity results indicate that the $N_2$ bubbling decreased the reaction rate constant, while the $O_2$ bubbling enhanced the reaction rate constant. This is possibly because the added $O_2$ molecules can react with electrons captured on the metal surface to form more $O_2^{\bullet-}$ active species for the photocatalytic reaction (Kim *et al.*, 2002), leading to the photocatalytic activity enhancement.

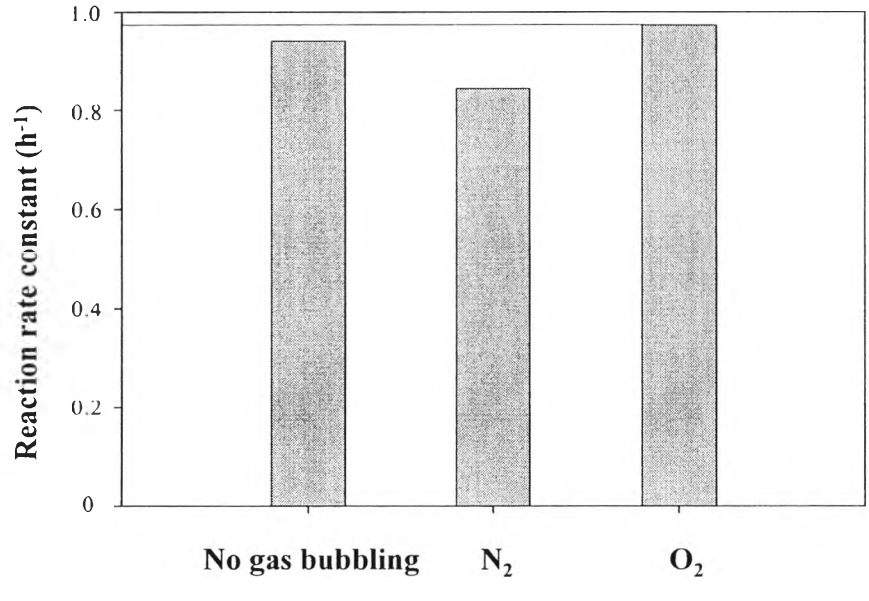


**Figure 4.18** Effect of dissolved oxygen on the reaction rate constant for phenol degradation of the synthesized 0.5 wt.% Pt-loaded mesoporous-assembled $SrTi_{0.97}Zn_{0.03}O_3$ photocatalyst calcined at 700 °C (Photocatalyst, 1 g; total reaction mixture volume, 200 ml; initial phenol concentration, 40 mg/l; and irradiation time, 4 h).